Quantitative Molecular Imaging in Living Cells via FLIM

Ching-Wei Chang and Mary-Ann Mycek

Abstract Fluorescence lifetime imaging microscopy (FLIM) employs fluorophore lifetime, rather than fluorescence intensity, for image contrast. Compared to intensity-based methods, lifetime imaging requires less calibration and/or correction for fluorophore concentration variations, photobleaching, and other artifacts that affect intensity measurements. We describe FLIM applications to probe the microenvironments of endogenous and exogenous fluorophores, including measurements of cellular metabolic co-factors, intracellular and extracellular oxygen, and molecular interactions via Förster resonance energy transfer (FRET). Several applications of FLIM for quantitative, live cell imaging are presented, including studies of cellular metabolic pathways, improved FRET detection of oncogene association, microfluidic bioreactor characterization for continuous cell culture, and improved analysis of FLIM images including image restoration and precision enhancement.

1 Introduction

The applications of fluorescence to biological sciences have been growing. During the past two decades, cellular and molecular responses in living cells have been determined by fluorescence measurements, and fluorescence has also been used for environmental monitoring, clinical chemistry, DNA sequencing, genetic analysis by fluorescence in situ hybridization (FISH), cell identification and sorting in flow cytometry, and revealing the localization and movement of intracellular substances in cellular imaging [1].

Steady-state or intensity-based fluorescence measurements are routinely employed for studies in cell biology. However, these measurements are sensitive to intensity-based artifacts such as excitation intensity variation, detection gain, optical

C.-W. Chang • M.-A. Mycek (✉)
Department of Biomedical Engineering, University of Michigan, Ann Arbor, MI, USA
e-mail: mycek@umich.edu

C.D. Geddes (ed.), *Reviews in Fluorescence 2010*,
Reviews in Fluorescence, DOI 10.1007/978-1-4419-9828-6_8,

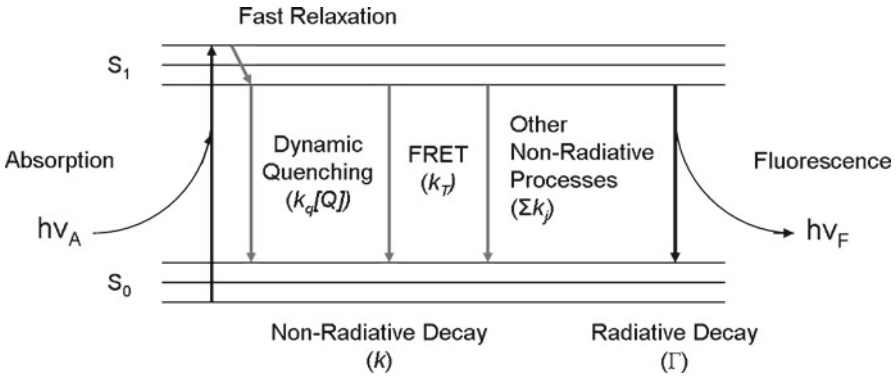

Fig. 1 A simplified version of the Jablonski diagram. Excited fluorophores can return to the ground state via a radiative decay process characterized by rate constant Γ and nonradiative decay processes characterized by k_q (bimolecular quenching constant), [*Q*] (quencher concentration, see section on "Oxygen Sensing via Dynamic Quenching"), k_T (energy transfer rate constant, see section on "FRET Detection of Molecular Interactions in Living Cells"), and k_j (rate constant for nonradiative processes other than dynamic quenching and FRET) [2]. Reproduced with permission from Elsevier Inc

loss, sample fluorophore (fluorescence molecule) concentration variation, photobleaching (damage of molecules due to light excitation), and microscope focusing. Further, fluorophores with similar spectral properties may be difficult to distinguish in fluorescence intensity imaging.

Recently, fluorescence lifetime measurements have become very popular in biological applications, and it has advantages over intensity-based measurements [1, 2]. Fluorescence lifetime, characterizing how fast the excited fluorescent molecules decay to the ground state, is an intrinsic property of fluorophores, depending only on the micro-environmental conditions such as temperature, pH, and interactions with other molecules. It is relatively insensitive to the factors affecting intensity, and therefore can serve as an indicator of fluorophores' micro-environment.

As an example, photobleaching can be an important issue in live-cell fluorescence measurement. Although photostable fluorophores, such as quantum dots, are becoming popular in fluorescence applications, organic molecules are still mostly used in live-cell applications. For example, green fluorescent proteins and its variants [3, 4] are very commonly used since they can be encoded with the proteins of interest to detect their levels of expression, localization, and interactions with other proteins as cells are responding to various environmental stimulations. However, fluorescent proteins can be vulnerable to photobleaching. Although researchers have been working to create more photostable fluorescent proteins and appropriate correction procedures to compensate for photobleaching [5], using fluorescence lifetime imaging microscopy (FLIM) is another way to circumvent this problem, since photobleaching affects intensity-based measurement but in most cases does not affect lifetime-based measurement.

A simplified Jablonski diagram is shown in Fig. 1. The ground and the first-excited electronic states are represented by S_0 and S_1, respectively. The horizontal

lines in each state represent different vibrational states of the fluorophore. In condensed phases (solid or liquid phase), after the absorption of photons, almost all fluorophores rapidly relax to the lowest vibrational state of the first-excited state. Then, there are two kinds of decay processes via which fluorophores can return to the ground state: nonradiative decay and radiative decay, which are characterized by the rate constants k and Γ, respectively, as shown in Fig. 1. Γ depends on the electronic properties of an isolated fluorophore, while k takes molecular interactions into consideration, such as dynamic (or collisional) quenching and Förster resonance energy transfer (FRET). Although only radiative decay is responsible for fluorescence emission, both nonradiative and radiative decays depopulate fluorophores in the first excited state (with population $N(t)$) and the decay of fluorescence emission intensity (proportional to $N(t)$) is attributed to both decay rates. In the simplest case, the decay is stochastic and hence appears exponential, as shown in (1) and (2).

$$\frac{\mathrm{d}N(t)}{\mathrm{d}t} = -(\Gamma + k)N(t) \tag{1}$$

$$N(t) = N_{\mathrm{o}}\mathrm{e}^{-(\Gamma+k)t} = N_{\mathrm{o}}\mathrm{e}^{-t/\tau} \tag{2}$$

where N_{o} is the initial number of fluorophores in the first excited state, and

$$\tau = \frac{1}{\Gamma + k} \tag{3}$$

is the fluorescence lifetime, which can be defined as the average time a fluorophore stays in the first excited state. As shown in (3), both decays play a role in lifetime.

Combining lifetime measurement with microscopy, FLIM produces spatially resolved images of fluorescence lifetime, providing another dimension of quantitative information for visualizing fluorophore responses. FLIM can be used with various microscopy techniques for different applications, and greatly helps reveal subcellular environmental changes in live cells and provide better detection of localization of molecular interactions.

For example, FLIM can be combined with wide-field parallel pixel detection and confocal sectioning utilizing spinning Nipkow disc microscopy to provide high-speed imaging [6], or combined with multifocal multiphoton excitation and time-correlated single photon counting to achieve 3D fluorescence lifetime imaging [7]. Also, the implementation of FLIM using a 40-MHz pulse train derived from a supercontinuum source for excitation, termed multiharmonic FLIM (mhFLIM), has been demonstrated [8] to accurately resolve bi-exponential decays of fluorophores without any a priori information.

FLIM applications are varied and include imaging astrocytic calcium homeostasis in a mouse model of Alzheimer's disease [9], helping large-scale, kinetic modeling

of molecular mechanisms using systems biology approaches [10], allowing for the discrimination of important biochemical features involved in atherosclerotic plaque instability and rupture [11], and have been suggested for single-molecule fluorescence experiments [12]. Comparison between healthy subjects and patients suffering from eye diseases such as age-related macular degeneration in early stage has also been performed using autofluorescence lifetime measurements [13, 14].

In this chapter, we describe the concept of a wide-field time-gated FLIM system and illustrate its applications to quantitative live-cell imaging, including studies of cellular metabolic pathways, improved FRET detection of oncogene association, microfluidic bioreactor characterization for continuous cell culture, and improved analysis of FLIM images.

2 Time-Gated Fluorescence Lifetime Imaging Microscopy

2.1 Concept

FLIM measures fluorescence lifetime and provides lifetime maps using various microscopy techniques, including wide-field, confocal, and multiphoton systems. While scanning confocal or multiphoton microscopy can be combined with FLIM for better light penetration ability and higher resolution, higher focused light energy and longer dwell time for excitation may cause cell damage and irresolvable spatial and temporal features in cellular responses due to cell movement during measurements. These problems could be even worse since shorter laser pulses such as those of femto-second lasers are usually needed in these applications.

On the other hand, wide-field time-gated FLIM (Fig. 2) can be used for high-speed imaging with fluorescent lifetime as image contrast. It can be achieved with a gating device such as a gated charge-coupled device (CCD) for recording gated, integrated fluorescence signals [16–19]. Time-gated FLIM provides high-speed snap shots of lifetime distributions because no laser scanning is required. In addition, it has advantages such as reducing light delivery into live cells. Therefore, the use of wide-field time-gated FLIM can reduce or remove the problems mentioned above.

2.2 Instrumentation

We previously designed and characterized a novel wide-field, time-domain FLIM system with picosecond resolution [20]. A nitrogen laser is used in this system to pump a dye laser for wide-range excitation (UV–visible–NIR). The large temporal dynamic range (750 ps – infinity), the 50-ps lifetime discrimination, and the spatial resolution of 1.4 μm of the system make it suitable for studying endogenous and exogenous fluorophores [20].

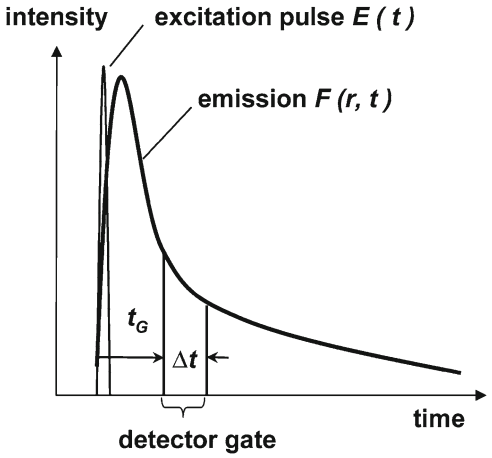

Fig. 2 Time-gated FLIM concept and an illustration of fluorescence decay. The system captures the fluorescence emission image at a delay time t_G after the excitation over an interval Δt by using a gated ICCD camera. Using intensity images captured at several t_G, a fluorescence lifetime image is constructed. *t*: time; *r*: spatial location [15]. Reproduced with permission from Springer-Verlag

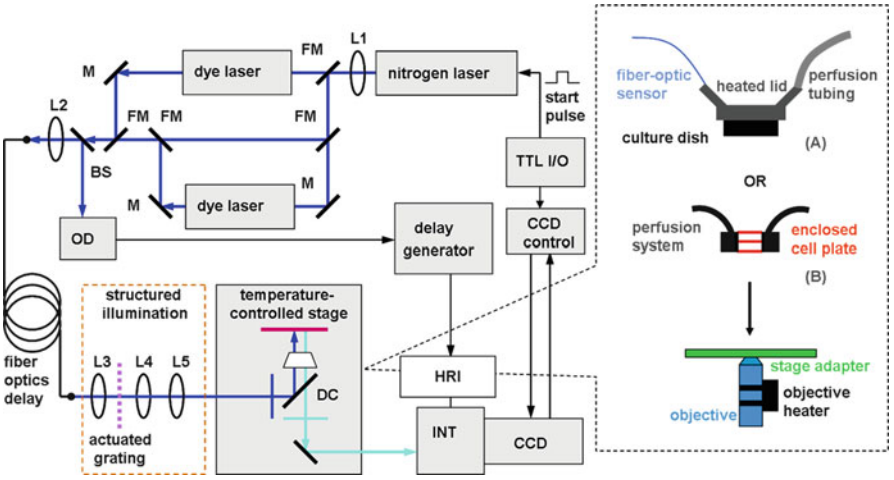

Fig. 3 Setup of the FLIM system. Depending on the laser dye used, this system can excite samples in the UV-NIR range (337–960 nm). Perfusion chamber and temperature control units provide physiological conditions for live-cell studies (see section on "Results: Physiological FLIM"). *CCD* charge-coupled device, *HRI* high-rate imager, *INT* intensifier, *TTL I/O* TTL input/output card, *OD* optical discriminator, *BS* beam splitter, *DC* dichroic mirror, *FM* mirror on retractable "flip" mount, *L1, L2, L3, L4, L5* quartz lenses, *M* mirror. *Thick (blue and cyan) solid lines* represent light path, while *thin (black) solid lines* represent electronic path [21]. Reproduced with permission from Optical Society of America

Figure 3 illustrates the instrumentation of our FLIM system. The excitation light was delivered via an optical fiber to an inverted microscope (Axiovert S100 2TV, Zeiss, Germany). A reference pulse split from the excitation light was sent to an optical discriminator to generate an electronic pulse, to be further sent to a picosecond delay generator (DEL350, Becker & Hickl, Germany), providing a time reference. The delay generator output was then used to trigger the gated intensified CCD (ICCD)

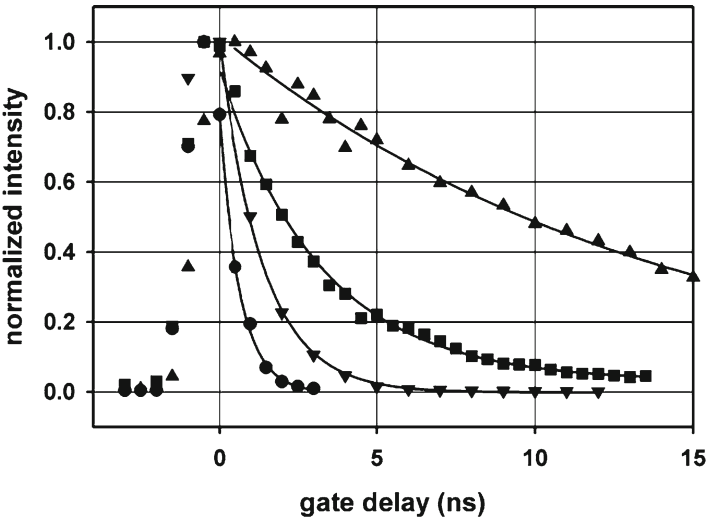

Fig. 4 Measured fluorescence intensity decays by using the FLIM system for fluorophores with a range of lifetimes (0.6–14 ns) including (*circle*) rose bengal, (*triangle pointing down*) POPOP, (*rectangle*) fluorescein, and (*triangle pointing up*) 9-cyanoanthracene. Excitation was at 337.1 nm. Single-exponential fits to the decay are represented by *solid lines* [15]. Reproduced with permission from Springer-Verlag

camera (Picostar HR, LaVision, Germany). The ICCD had variable intensifier gain and gate width settings varying from 200 ps to 10 ms and can be used to implement high-speed imaging in other applications as well [22].

The temporal profiles of fluorescent molecules of known lifetimes were measured with the system to evaluate the system's ability to distinguish different lifetimes. Rose bengal (5×10^{-5} M in ethanol), POPOP (saturated in ethanol), fluorescein (10^{-5} M in de-ionized water), and 9-cyanoanthracene (8×10^{-5} M in ethanol) ranging in lifetimes from 0.6 to ~14 ns were measured (Fig. 4) [15]. Lifetimes were determined with a least-square method for single exponential decays (see section on "Data and Image Processing"). The lifetime values determined with the FLIM system showed excellent agreement with those measured independently using a nitrogen laser-based fluorescence lifetime spectrometer (FLS) [23].

2.3 Key Features of Lifetime Sensing

Fluorescence lifetime is an intrinsic property of fluorophores and is insensitive to intensity artifacts, such as photobleaching and variation in sample fluorophore concentration, as described previously in "Introduction". On the other hand, due to the fact that lifetime is affected by the nonradiative decay process [Fig. 1 and (3)], it is sensitive to the fluorophore's micro-environment, including factors such as

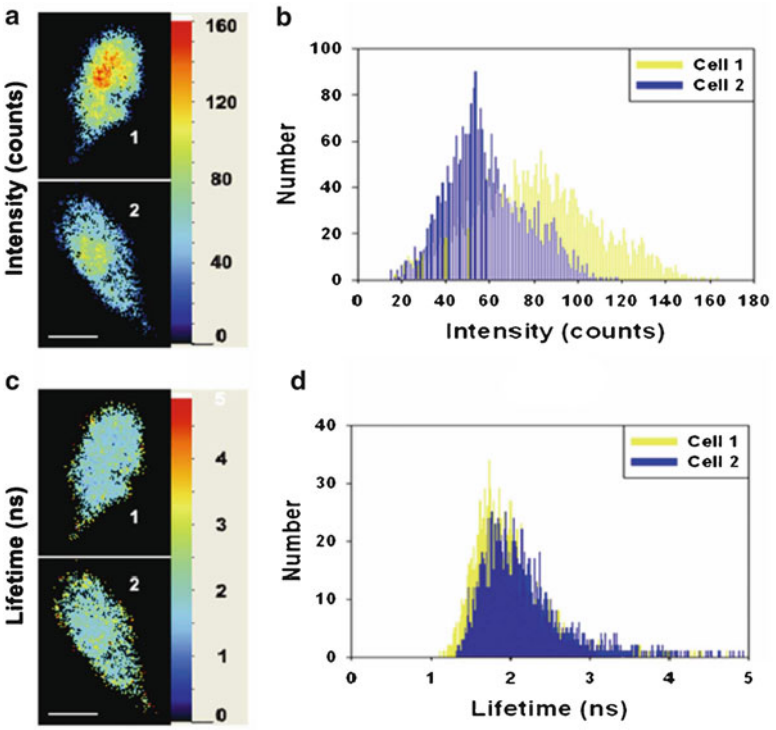

Fig. 5 ECFP fluorescence of live CV1 cells transfected with ECFP-RhoGDIγ + EYFP-RhoC (see section on "Oncogene RhoC and Its Interactions" for more details). The intensity histogram (**b**) and the corresponding image (**a**) show that the distribution of inter- and intracellular ECFP fluorescence was heterogenous, while the lifetime histogram (**d**) and the corresponding image (**c**) exhibit far smaller variability. The *scale bar* represents 20 μm [16]. Reproduced with permission from Optical Society of America

temperature, pH, oxygen concentration, polarity, molecular associations (binding), ion concentration, and relaxation through collisional (dynamic) quenching and fluorescence resonant energy transfer (FRET) [2].

Figure 5 demonstrates the insensitivity of lifetime to the difference in plasmid uptake and expression in a live-cell experiment. In this example, fluorescent proteins enhanced cyan fluorescent protein (ECFP) and enhanced yellow fluorescent protein (EYFP) were used to detect live-cell interactions between Ras Homology Protein C (RhoC) and Rho Guanine nucleotide Dissociation Inhibitor gamma (RhoGDIγ) via FRET (more details are described in "Oncogene RhoC and Its Interactions" and Fig. 13). Figure 5 shows ECFP fluorescence intensity image (a) and lifetime image (c) of living CV1 cells transfected with ECFP-RhoGDIγ + EYFP-RhoC. The intensity image and the corresponding histogram (b) show broad intracellular ECFP fluorescence distributions. Moreover, intercellular variability can be clearly observed by the two distinct distributions. On the other hand, the lifetime image and the corresponding histogram (d) exhibit far smaller intra- and intercellular variability [16].

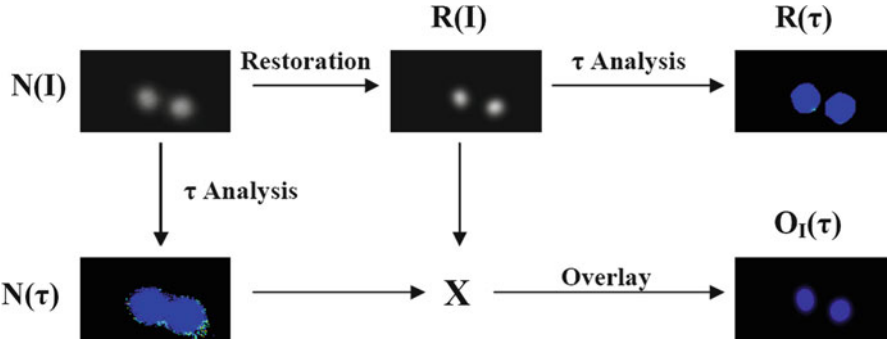

Fig. 6 Image processing techniques used to enhance the quality of lifetime maps. $N(\mathrm{I})$: native intensity image; $N(\tau)$: native lifetime image; $R(\mathrm{I})$: restored intensity image; $R(\tau)$: restored lifetime image; $O_{\mathrm{I}}(\tau)$: intensity-overlay lifetime image [28]. Reproduced with permission from Optical Society of America

2.4 Data and Image Processing

Fluorescence lifetime maps can be constructed rapidly with an analytic least squares lifetime determination algorithm using four gates (see Fig. 2) on a pixel-by-pixel basis [25–27]:

$$\tau_p = -\frac{N\left(\sum t_i^2\right) - \left(\sum t_i\right)^2}{N\sum t_i \ln I_{i,p} - \left(\sum t_i\right)\left(\sum \ln I_{i,p}\right)} \tag{4}$$

where τ_p is the lifetime of pixel p, $I_{i,p}$ is the intensity of pixel p in image i, t_i is the gate delay of image i, and N is the number of images. All sums are over i.

Further image processing techniques can be used to enhance the quality of lifetime maps. For example, image restoration and/or deconvolution can be used to remove the optical distortion during microscopic imaging. The point spread function of the imaging system, which can be defined as the image of an infinitely small point source (or a delta function), is assumed to convolve and distort the original image. If the four-gate protocol mentioned above is used, each of the four-gated intensity images can be restored before lifetime mapping.

Figure 6 is an illustration of the effect of intensity and lifetime image restoration on 3-μm-diameter yellow–green (YG) fluorescent microspheres (Polysciences, Warrington, PA) [28]. The haze in the native intensity image $N(\mathrm{I})$ leads to the native lifetime image $N(\tau)$ where the two spheres are indistinguishable. On the other hand, higher signal-to-noise ratio can be observed in the restored intensity map $R(\mathrm{I})$, especially in the central regions of the spheres, which in turn leads to the reduction in haze and distinguishable spheres in the restored lifetime map $R(\tau)$.

Quantitatively, there is only a 3% change in lifetime (from 1.65 to 1.60 ns) and the sphere diameter is reduced from 4.81 μm in the native intensity image to 3.35 μm in the restored intensity image, making it closer to the actual sphere size [28].

Figure 6 also demonstrates another data-processing technique called "intensity-overlay restoration" for the same 3-μm YG microsphere sample. In the approach, both the native lifetime map (color coded) and the restored first-gate intensity image (in grayscale) were generated and then combined via multiplication to yield a single intensity-overlay lifetime map. In this approach, fluorophore intensity and lifetime can provide complementary information; while lifetime indicates the fluorophore micro-environment, intensity provides concentration and cell morphological information. In addition, intensity-overlay restoration produces no lifetime change [28].

Another crucial issue is the precision of lifetime determination in FLIM. When using high-intensity light sources such as lasers for sample excitation, it is essential to ensure that live-cell systems remain undisturbed. Therefore, in biological applications of FLIM, when minimizing potential cell damages due to excitation light, low fluorescence signals from samples can be a challenge, which may cause poor precision in lifetime determination.

To improve FLIM precision, optimal gating can be implemented [29]. Alternatively, image "denoising" (noise removal) has also the potential to improve the precision of fluorescence images [30–32]. These image denoising techniques include total variation (TV) methods [29, 33, 34], wavelet analysis [30, 31], non-parametric regression method [35], and multiframe SURE-LET (Stein's unbiased risk estimate-linear expansion of thresholds) denoising [36].

Recently, we reported novel TV models with the capability to remove both Poisson noise and non-Poisson-distributed, varying magnitudes of noise. Studies have illustrated the applications of these novel TV models to FLIM and demonstrated that they not only can improve the precision of FLIM by greater than fivefold [29, 34] but also show promising results to better denoise low-light live-cell FLIM images than wavelet-based methods [33].

3 Oxygen Sensing via Dynamic Quenching

3.1 Concept

Knowledge of intracellular oxygen levels can significantly help us understand numerous cellular processes. For example, oxygen in cell cultures influences cell signaling, growth, differentiation, and death [37]. Although there is a variety of techniques for live-cell and tissue oxygen measurement, including Clark-type electrodes, fluorescence, electron paramagnetic resonance (EPR), and nuclear magnetic resonance, noninvasive measurements with high sensitivity and spatial resolution are achievable only by using fluorescence-based measurements [38].

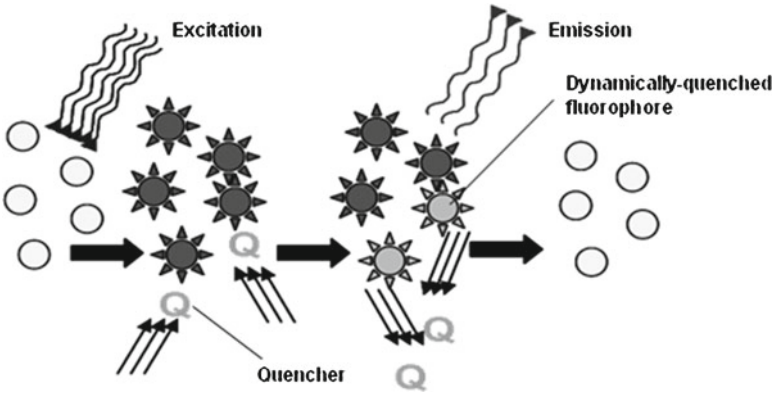

Fig. 7 During the decay process, dynamic quenching happens when quenchers collide with excited-state fluorophores, deactivate them, and shorten their detected lifetime [2]. Reproduced with permission from Elsevier Inc

Ruthenium(II)-complex-based fluorescence probes have been used for intracellular oxygen sensing, whose principle is fluorescence quenching by oxygen and has been used in both intensity-based measurements [39, 40] and lifetime-based measurements [41–43]. Fluorescence quenching can be defined as any physical process causing decrease in fluorescence intensity [44]. The type of quenching process where oxygen molecules are involved is dynamic (or collisional) quenching. The concept of dynamic quenching is shown in Fig. 7. Dynamic quenching happens during the decay process, when quenchers deactivate excited-state fluorophores. The deactivated fluorophores will therefore follow nonradiative decay process (see Fig. 1) leading to a quicker decay of fluorescence and hence a shorter lifetime [2].

Because intensity-based fluorescence measurements will detect all quenching mechanisms including static quenching and losses due to scattering, lifetime-based fluorescence measurements, which are insensitive to other forms of quenching, can specifically indicate dynamic quenching [44]. One advantage of fluorescence lifetime methods, as mentioned previously, is the insensitivity to fluorophore concentration variations, thereby minimizing these artifacts [40].

3.2 Calibration

Here, we briefly describe the calibration of a ruthenium(II)-complex-based fluorescence probe. One of the ruthenium(II)-complex-based fluorescence probes for intracellular oxygen sensing is ruthenium tris(2,2′-dipyridyl) dichloride hexahydrate (RTDP), which has been studied for its photophysical and photochemical properties [38]. The advantages of using RTDP include a long fluorescence lifetime (hundreds of nanoseconds), easy uptake by cells, and minimal cytotoxic and phototoxic effects [21].

Temperature control is required in lifetime-based oxygen sensing. Measurements made with the FLIM system indicated that RTDP lifetime decreased linearly as temperature increases [21]:

$$\tau = -4.4975 \times T + K, r^2 = 0.9867 \tag{5}$$

where τ = lifetime and T = temperature in degree Celsius and K was a constant.

With temperature fixed at 37°C, the results of RTDP calibration indicated a linear relationship between oxygen levels and relative lifetime (defined as the ratio of uninhibited RTDP lifetime (τ_0) to τ_x at a given oxygen level $[O_2]_x$) [21], which was in good agreement with the Stern–Volmer equation (Fig. 8):

$$\frac{\tau_0}{\tau_x} = 1 + K_q [O_2]_x \tag{6}$$

where K_q is the Stern–Volmer quenching constant. K_q was evaluated over multiple runs to be $4.5 \pm 0.4 \times 10^{-3}$ μM^{-1}, which is higher than other reported values measured at room temperature, confirming that K_q increases with temperature [42].

3.3 Live-Cell Results

The FLIM system was used for the studies of metabolic function in two related cell lines: normal human squamous esophageal epithelial cells (HET) and Barrett's adenocarcinoma esophageal cells (SEG). Both cell lines were imaged for NAD(P)H (see section on "Endogenous Fluorescence Measurements in Living Cells") and assessed for oxygen levels [21].

Figure 9b–e shows the images, including the maps of lifetime and oxygen levels, of SEG cells, which were used as a model cell line to assess the capability of RTDP for intracellular oxygen sensing. The cell positions (b) overlap with RTDP fluorescence (c). The fluorescence intensity image (c) is nonuniform, due to differential uptake of RTDP, while the lifetime map (e) shows much higher uniformity, reflecting the insensitivity of lifetime to intensity-based artifacts and demonstrating similar oxygen levels. An oxygen level map (d) was generated with the RTDP calibration curve (Fig. 8), indicating uniform oxygen levels of approximately 285 μM, which is higher than the reported in vivo values $[O_2]_{SEG} = 260.16 \pm 17$ μM due to the fact that 285 μM was observed ex vivo and is indeed consistent with the values previously obtained in such measurements [42, 45]. This is a leap forward from measurements of extracellular oxygen alone to those of intracellular oxygen, since gradients between extra- and intracellular spaces cannot be explained by simple diffusion rates alone [46].

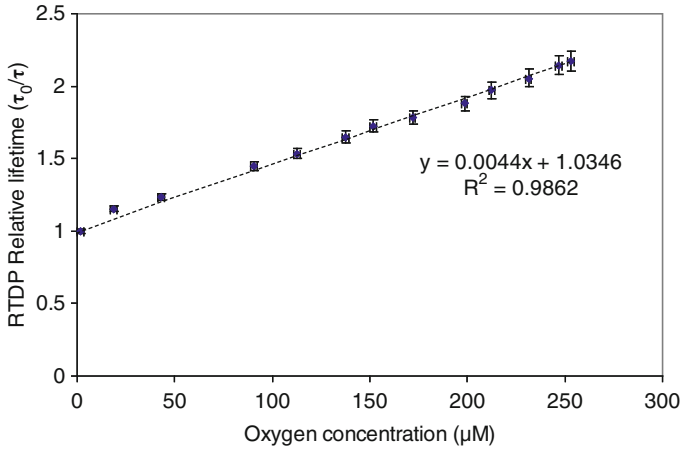

Fig. 8 RTDP calibration curve, indicating a linear relationship between oxygen levels and relative lifetime, could differentiate oxygen levels by as little as 8 μM [21]. Reproduced with permission from Optical Society of America

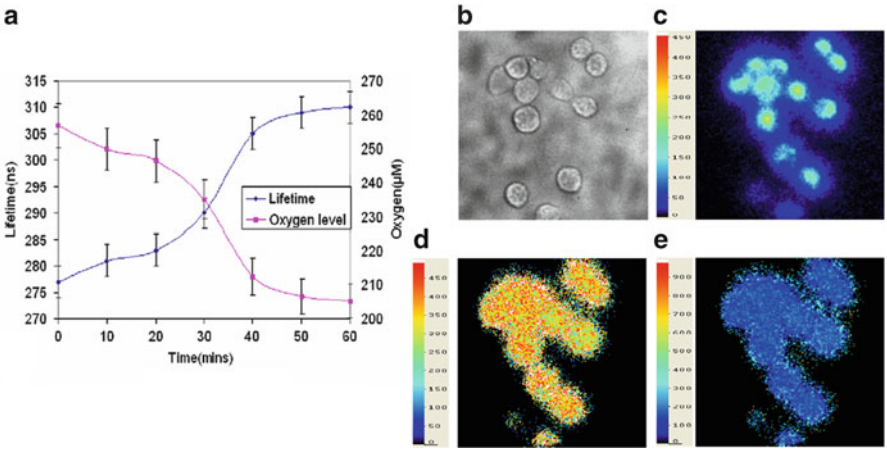

Fig. 9 (**a**) Depletion experiment results on SEG (see text). Images of SEG incubated with RTDP: (**b**) DIC, (**c**) fluorescence intensity in counts, (**d**) oxygen in μM, and (**e**) lifetime in ns. In the time lapse between the two images (**b**) and (**c**), one cell in the bottom shifted position [21]. Reproduced with permission from Optical Society of America

Further experiment involving 1-h time-lapse FLIM measurements was made on SEG to verify that the increase in RTDP lifetime (~35 ns) would indicate decrease in oxygen levels (~50 μM) due to cellular consumption (Fig. 9a).

The novel protocol for accurate intracellular oxygen sensing via FLIM was also validated with EPR, which provided a "gold standard" for intracellular oxygen estimation. Oxygen concentrations were evaluated in live HET and SEG cells, and there was a good agreement between oxygen levels derived from the FLIM protocol and EPR [47].

3.4 Applications to Microfluidic Bioreactors

The use of microfluidic devices in cell-based assays and microscale tissue engineering provides the capability of manipulating spatiotemporal conditions. For example, poly(dimethyl siloxane)-(PDMS)-based microfluidic systems can be used as biocompatible and rapidly prototyped systems for microscale-cell culture. In this case, an extracellular fluid-to-cell (volume) ratio close to the physiological value [37] of 0.5 could be achieved with continually perfused conditions, and this may be critical in cell fate specification in developing tissues. Therefore, it is important to characterize the components (e.g., mitogens, nutrients, oxygen) that influence cellular responses in microfluidic bioreactors quantitatively with minimal perturbation [48].

PDMS bioreactors are popular due to their high diffusivity of oxygen, which has been repeatedly demonstrated [49]. However, it has been demonstrated [50] that the diffusivity of PDMS can vary due to protein adsorption or surface modification, and this variability, along with cellular uptake and culture media perfusion, could affect spatial variations in oxygen within PDMS bioreactors.

For the applications to bioreactor systems, there are advantages of fluorescence-based oxygen sensing agents over more traditional, electrode-based approaches: they are well suited for small volumes, are relatively nonperturbing to the system setup, and do not cause additional oxygen consumption during the measurement. Fluorescence-based oxygen sensing enables time-lapse studies (hours or days) without disturbance, as well as imaging spatial oxygen distributions in long-term cell culture.

As an example of the application of FLIM to oxygen sensing in microfluidic bioreactors, a PDMS cell culture device with six loops is illustrated in Fig. 10a. The device was small and transparent, making it ideal for microscopic analysis. Figure 10b shows the FLIM images of RTDP, indicating oxygen levels at different points along each loop. The FLIM images demonstrated that oxygen levels differed by as much as 20% within a loop, which was consistently observed across multiple devices. In addition, these differences were statistically significant [48]. Furthermore, studies were also conducted to combine computerized microfluidics, in situ oxygen sensing with FLIM, and mathematical models to analyze oxygen gradients induced by cellular uptake in microfluidic bioreactors. This leads to new opportunities for microphysiologic studies utilizing oxygen gradients and low oxygen tensions [51].

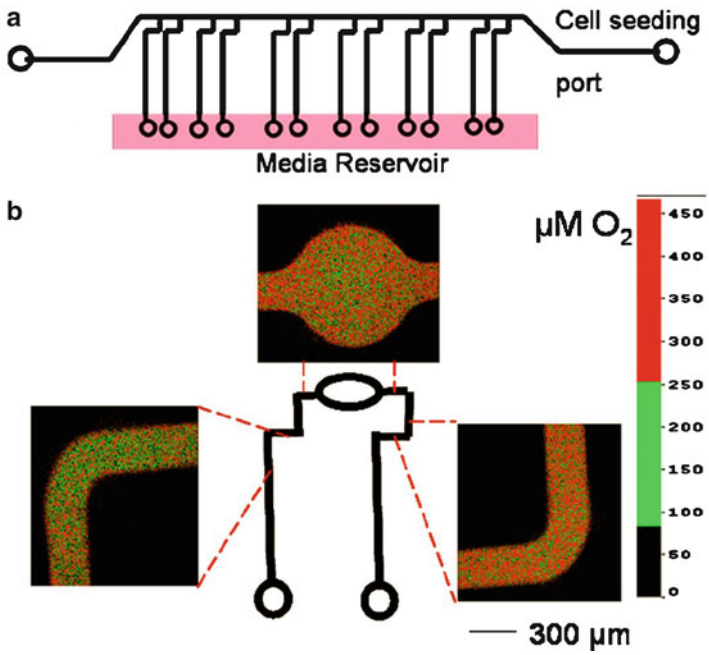

Fig. 10 FLIM-based oxygen measurements from a closed-loop PDMS bioreactor with continuous C2C12 mouse myoblasts cell culturing. (**a**) Device schematic. (**b**) Images of oxygen concentration at different points in binary scale in μM [48]. Reproduced with permission from SPIE

4 Endogenous Fluorescence Measurements in Living Cells

Fluorescent molecules intrinsic to biological cells and tissues, or endogenous fluorophores, can be used as potential probes of metabolic function, tissue morphology, and biomarkers of disease [52]. Endogenous fluorophores commonly used in these studies include amino acids (tryptophan, tyrosine, phenylalanine), coenzymes (NAD(P)H, flavins), and structural proteins (collagen, elastin). Unlike exogenous fluorophores, endogenous fluorescence measurements raise no concerns for contrast agent toxicity or delivery. Again, intensity-based endogenous fluorescence methods are complemented with lifetime-based measurements for disease detection and metabolic imaging (reviewed in [53]).

Endogenous fluorescence lifetimes in cellular studies have focused on metabolism monitoring. For example, Lakowicz et al. [54] simultaneously distinguished free and protein-bound NADH lifetimes in solution using frequency-domain fluorescence lifetime imaging, where samples were simultaneously excited at 355 nm and detected using a gain modulated ICCD. A difference between mean lifetimes of 0.4 ns (free state) and 1 ns (protein-bound state) were distinguished. In another example, Schneckenburger and König [55] studied respiratory deficient and intact

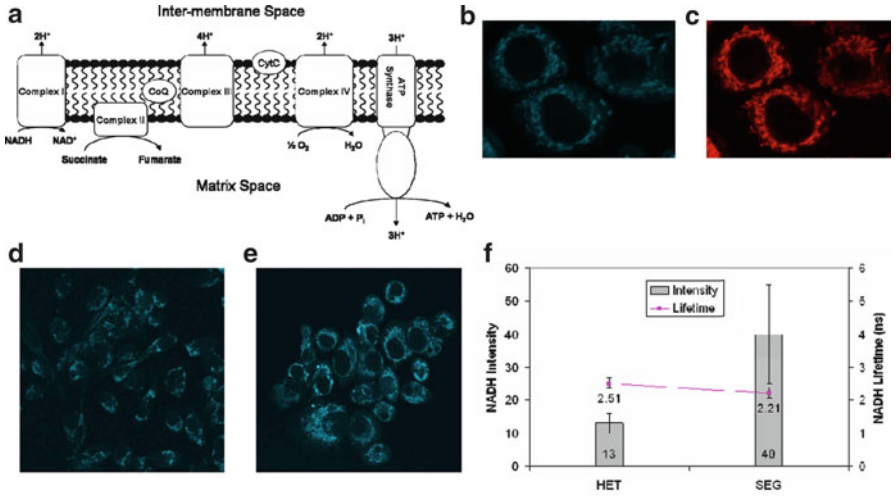

Fig. 11 (**a**) Mitochondrial oxidative phosphorylation, (**b**) fluorescence of NADH, and (**c**) images of Mitotracker-stained SEG. Excitation was at 543 nm and emission was at 636 nm for the Mitotracker. Mitotracker Red is used for mitochondria tracking in live cells. Fluorescent signals from both markers co-localized. Confocal images of fluorescence intensity of NADH in HET (**d**) and SEG (**e**). The SEG consistently exhibited a brighter signal compared to the HET by ~2.5-fold. (**f**) Plot of differences in intensity and lifetime of NADH fluorescence between the HET and SEG over multiple FLIM measurements. No statistically significant differences were observed in the lifetime [21]. Reproduced with permission from Optical Society of America

strains of *Saccharomyces cerevisiae* (Baker's yeast) with lifetime imaging of NAD(P)H and flavins as metabolic indicators.

Figure 11 demonstrates the detection of NADH for the indication of the difference in metabolic functions in oxidative phosphorylation, which can provide a perspective on cancer progression [21]. One of the first steps in oxidative phosphorylation involves complex I reducing NADH to NAD+ along with electron transfer to the carrier coenzyme Q (CoQ) (Fig. 11a). Figure 11 shows confocal microscopic fluorescence intensity images of SEG (Barrett's adenocarcinoma esophageal cells) incubated with a commercial mitochondrial stain (Mitotracker Red). A comparison of Fig. 11b, c indicates that the Mitotracker fluorescence and the NAD(P)H fluorescence have the same origin, which in turn demonstrates that mitochondrial NADH, not NADPH, contributed the observed fluorescence. Figure 11d, e further provides confocal images of NADH fluorescence intensity from HET (normal human squamous esophageal epithelial cells) and SEG, respectively, under the same settings. Brighter fluorescence intensity of SEG can be easily observed, with a statistically significant difference ($p<0.05$, Fig. 11f) versus the fluorescence intensity of HET.

FLIM measurements were made for NADH in both cell lines with obtained lifetime values $\tau_{HET}=2.51\pm0.16$ and $\tau_{SEG}=2.21\pm0.16$ ns, which are within the range of values reported in literature [54]. However, this difference in lifetime values was

not statistically significant, indicating that the previously mentioned fluorescence intensity differences between the HET and the SEG could only be attributed to differences in intracellular NADH levels, not the NADH micro-environment. This observation of higher NADH levels in esophageal cancer cells than in normal esophageal cells could explain the reported higher NAD(P)H levels in dysplastic versus nondysplastic esophageal tissues via clinical studies [56].

5 FRET Detection of Molecular Interactions in Living Cells

5.1 Concept

Förster (or fluorescence) resonance energy transfer (FRET) is sometimes referred to as an in vivo "nanoscale ruler," to measure the distance similar to the sizes of biological macromolecules, such as the protein diameter, live-cell protein interaction distance, and biological membrane thickness. FRET can be used to measure the distance between two fluorophores, two sites on a macromolecule, and two molecules attached with fluorophores for the detection of the corresponding molecular interactions in live cells.

FRET theory was developed by Professor Theodor Förster [57]. At least one donor–acceptor (D–A) pair is required for FRET to occur, although more than one such pairs can be involved. For FRET to happen, overlap is needed for the donor emission spectrum and the acceptor excitation spectrum. When the donor and the acceptor are sufficiently close to each other, the energy absorbed upon donor excitation can be transferred to the acceptor nonradiatively (see Fig. 1; the nonradiative pathway without the re-emission of photon).

To quantify the distance for FRET to occur in a D–A pair, "Förster distance" is defined as the distance at which the energy transfer efficiency is 50%. The energy transfer efficiency (E) is defined as

$$E = \frac{k_T}{\tau_D^{-1} + k_T} \tag{7}$$

where τ_D is the donor lifetime in the absence of acceptor and k_T is the energy transfer rate from a donor to an acceptor. k_T is given by

$$k_T = \frac{1}{\tau_D}\left(\frac{R_0}{r}\right)^6 \tag{8}$$

where R_0 is the Förster distance and r is the donor–acceptor distance. When $r = R_0$, $E = 50\%$, which is the definition of Förster distance. What can also be observed is the highly nonlinear dependence of k_T on r.

D–A pairs with longer R_0 are usually preferred, because in this case FRET can be easier to detect. The typical value of R_0 is in the range of 20–60 angstroms. There are several factors that will affect Förster distance, for example, the extent of D–A spectra overlap, the relative orientation of D–A, the medium refractive index, and the quantum yield of the donor in the absence of acceptor. Among these factors, the relative orientation of D–A and the medium refractive index are typically regarded as constants for biomolecules in aqueous solutions. Therefore, R_0 is usually considered to be approximately fixed for a given D–A pair, since it is mainly dependent only on the optical properties of the fluorophore pairs.

FRET can be used to monitor any phenomena accompanied with changes in the D–A distance, such as macromolecule conformational changes, or enzyme cleavage of a macromolecule. In these cases, endogenous fluorophores, such as tryptophan and a ligand that binds to a ligand binding site, can serve as a D–A pair.

Exogenous fluorophores are also used as D–A pairs in cell biology. Examples are fluorescent proteins such as CFP, YFP, and their enhanced variants ECFP, cerulean, CyPet, EYFP, citrine, Venus, YPet. In this case, the donor and acceptor fluorophores are usually constructed with the proteins of interest in the DNA vectors. Either the N terminal or the C terminal of the proteins can be attached with the fluorophores. The vectors are then transfected or transduced into the model cells, which usually are cells easier for vectors to transfer, or cells related to the cells where the protein functions and interactions are of interest. Vector sizes may affect FRET, if vectors are not transferred efficiently [58, 59], producing weak signal-to-noise ratio, or if the ratio of transferred donor to acceptor is too high or too low.

Both fluorescent intensity and lifetime can be used to detect FRET. As shown in Fig. 1, k_T is an additional decay rate when the acceptor is present. This causes the donor lifetime to be shortened and the donor intensity lowered if FRET occurs. The extent of shortening/lowering depends on the D–A distance r. Although r can be fixed for labeled proteins, in solution or membranes, where the donors and acceptors can diffuse freely, r can vary, and it will be necessary to calculate an averaged k_T from the D–A spatial distribution. In addition, if a multi-exponential decay happens in the presence of different fluorophores or different environments, the averaged τ value over all exponential curves is required for the determination of FRET efficiency.

Detection of FRET has been implemented with intensity-based methods [60]. For example, sensitized emission of acceptor [61, 62], ratiometry of donor to acceptor intensities, donor dequenching with acceptor photobleaching, donor photoquenching with photoactivated acceptor [63], and stoichiometry FRET [64] have been demonstrated.

On the other hand, detection of FRET with FLIM can be highly favored over intensity-based methods for several reasons [2, 15, 65]. As an example, if detection of FRET efficiency of ~10% is desired, the inter- and intracellular variations in fluorescence emission intensity might need to be controlled to be very low, and this may not be easy for experiments with nonuniform transfection distributions. FLIM detection of FRET with $E = \sim 10\%$ allows intensity variations to be as high as 30% [24] or even higher, while still providing statistically very significant results (p-value $< 10^{-10}$) supporting the occurrence of FRET.

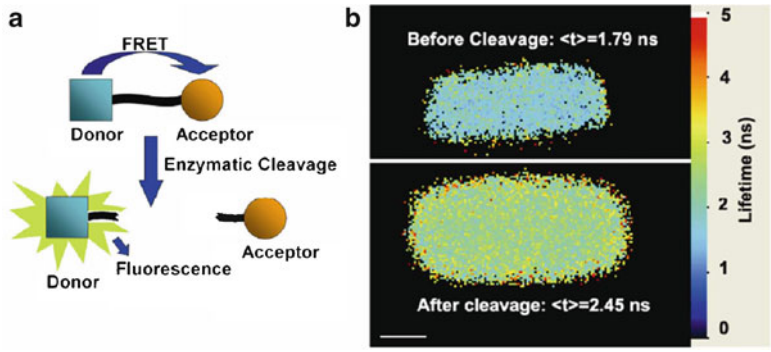

Fig. 12 A demonstration of FRET experiment in solution. (**a**) Concept of the use of FRET for monitoring the cleavage of a peptide substrate serving as a linker for FRET donor and acceptor. (**b**) Images of the donor fluorescence lifetime before (*upper*) and after (*lower*) cleavage. *Scale bar*: 50 μm [16]. Reproduced with permission from Optical Society of America

A FRET assay in solution is illustrated in Fig. 12a [16]. In Fig. 12b, it is demonstrated that the lifetimes of the substrate after the enzyme cleavage became higher versus before the cleavage. As mentioned previously in the section on "Instrumentation," our time-gated FLIM system with 50 ps lifetime discrimination can be used to detect this lifetime difference of 660 ps. Furthermore, the lifetime of the substrate after cleavage (2.45 ns) was close to the product standard lifetime (2.42 ns; with complete cleavage of the substrate), which demonstrates the ability of our FLIM system to detect FRET in a well-controlled system.

FRET-FLIM has already been widely used in biological applications [65–67]. Protein localization was characterized with a two-photon FRET–FLIM system [68], and FRET–FLIM was used to study plasma membrane organization in cowpea protoplasts [69]. A frequency-domain FRET–FLIM-based detection of localized phosphorylated protein was also conducted [70]. A table of commonly used FRET fluorophore pairs for FLIM studies was provided in a review paper [61].

The goal of the study in this section is to provide a better quantitative FRET detection of molecular interactions in living cells. We demonstrate that FRET can be better detected with FLIM than with intensity. The approaches described here also significantly help us to determine physiologically relevant interactions in living cells that can provide us with insight into treatments of diseases such as breast cancers mentioned in this section.

5.2 Live-Cell FRET: Intensity Versus Lifetime

Live-cell microscopic FRET detection is much more challenging compared to FRET detection in solution such as the one shown in Fig. 12. As a demonstration, several experiments were conducted in our laboratory to verify the insensitivity

of lifetime measurements to the effects of known intensity-based artifacts, such as difference in plasmid uptake and expression (see section on "Key Features of Lifetime Sensing" and Fig. 5), photobleaching, and variation in cell morphology. This was to ensure the reliability of the lifetime measurements of our previously used intracellular ECFP in the FRET experiments for the detection of live-cell RhoC and RhoGDIγ interactions (see section on "Oncogene RhoC and Its Interactions") [16].

In the case of photobleaching, two consecutive ECFP fluorescence measurements were taken on live cells to test the reproducibility of the measurements. The lifetimes of cells transfected with ECFP-RhoGDIγ + EYFP-RhoC were reproducible to 0.02%, while the intensities of these cells were only reproducible to 5%. Therefore, intensity measurements were much more affected by photobleaching than lifetime measurements [16].

The location of focal plane in microscopic imaging may play a role in the variations in the measurements. This issue was addressed by intentionally changing the objective focus slightly to demonstrate the relative insensitivity of lifetime measurements to small changes in the location of focal plane. Such slight change caused 2, 0, and 6% variation in ECFP fluorescence lifetime, versus 4, 3, and 26% variation in ECFP fluorescence intensity, for three live cells transfected with ECFP-RhoGDIγ + EYFP-RhoC [16].

5.3 Oncogene RhoC and Its Interactions

RhoC has been found to be a transforming oncogene for mammary epithelial cells and has been identified as a specific marker of aggressive breast cancers. Its activation can lead to a highly invasive, angiogenic, and metastatic phenotype, extremely akin to inflammatory breast cancer, which has very poor prognosis from its inception. However, the detailed biophysical mechanisms for activation and inhibition of it are not completely understood [71]. Therefore, it is critical to characterize molecular interactions of oncogene RhoC in the living cells in order to understand its behaviors and how it performs its functions as an oncogene, which will provide us valuable information when developing novel treatments toward inflammatory breast cancer.

RhoC and its isoforms RhoA and RhoB belong to the Rho family within the Ras GTPase superfamily. In its active state, RhoC is associated with GTP and localizes to the membrane, where it is capable of binding to its effectors and participating in the focal adhesion complex, to which microtubules converge [71]. When RhoC is inactive, it is associated with GDP and is able to bind with RhoGDIγ in the cytoplasm.

In order to study the molecular interactions of Rho GTPases, many researchers utilized FRET [72–75], or designed and optimized the FRET probes specifically for this group of proteins [76, 77]. In particular, some research groups used FLIM–FRET to study the Rho family [66, 78–80].

In the following section, we explore the molecular interactions of RhoC in living cells with FLIM–FRET experiments. To accomplish this, we studied a live-cell

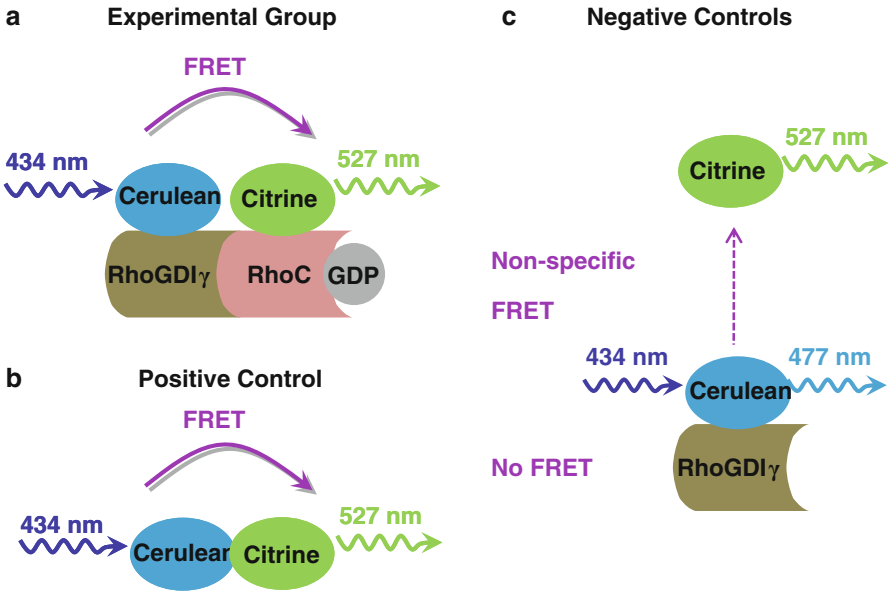

Fig. 13 FRET studies on the interactions between RhoC and RhoGDIγ. (**a**) Cerulean-RhoGDIγ + citrine-RhoC (the experimental group, with FRET). (**b**) Cerulean-citrine (the positive control, with FRET). (**c**) Cerulean-RhoGDIγ alone and cerulean-RhoGDIγ + citrine (negative controls, no FRET and nonspecific FRET, respectively). The wavelengths of fluorophore excitation and emission maxima are also labeled [24]. Reproduced with permission from SPIE

system involving RhoC inactive-form interactions. Interactions between RhoGDIγ and RhoC caused FRET to occur from the donor (cerulean, a further enhanced variant of CFP, attached to RhoGDIγ) to the acceptor (citrine, a further enhanced variant of YFP, attached to RhoC) in our experimental cellular group, as in Fig. 13a. In the positive control cellular group, Fig. 13b, cerulean was linked to citrine, and therefore FRET must occur. Two negative control cellular groups (Fig. 13c) were implemented: cerulean-RhoGDIγ alone, which had no FRET occurring, and cerulean-RhoGDIγ + citrine, which indicated nonspecific FRET. Living CV1 cells (monkey kidney epithelial cells) were either single- or double-transfected with the plasmids encoding corresponding fusion proteins using GeneJammer transfection reagent (Stratagene, La Jolla, California) [16].

5.4 Results: Physiological FLIM

We developed and applied a physiological FLIM system with experimental controls for CO_2 and temperature stabilization to create a physiological environment for live-cell FLIM studies. In Fig. 14, the donor lifetime values of the experimental cellular

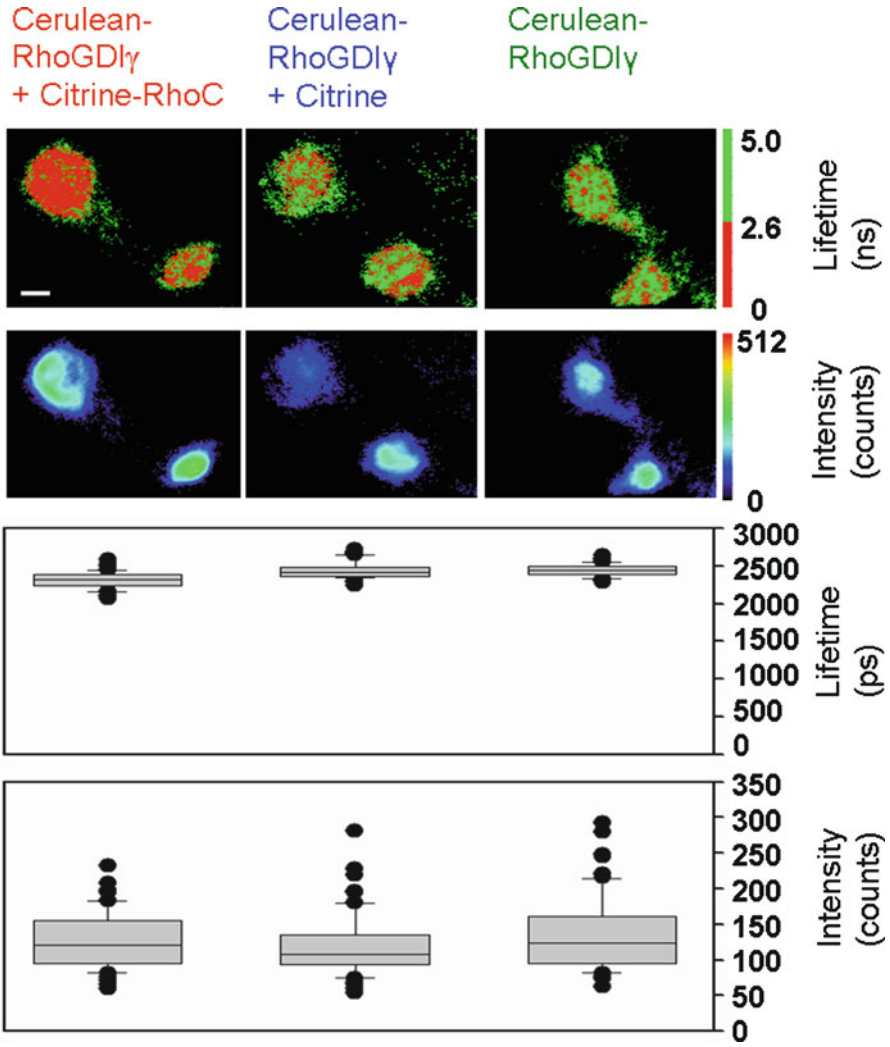

Fig. 14 Donor fluorescence lifetime versus intensity for live-cell FRET. Representative images (*top*) and box plots of intercellular distribution of the extracted values averaged per cell (*bottom*) for the experimental group (*left*) and the two negative controls (*middle* and *right*). FRET was indicated by the statistically significantly smaller donor lifetime values of the experimental group compared to the two negative controls (p-value $\leq 4.0 \times 10^{-10}$). This difference was not distinguishable by intensity measurements, due to higher inter- and intracellular variability (p-value > 0.18). *Scale bar*: 15 μm [24]. Reproduced with permission from SPIE

group were statistically significantly smaller than the two negative controls (p-value $\leq 4.0 \times 10^{-10}$), indicating FRET. Intensity images, however, exhibited many more inter- and intracellular variations, thereby obscuring the detection of any possible FRET (both specific and nonspecific) occurring in this system. When quantified

by relative standard deviation values obtained from the FRET data in Fig. 14, multifold improvement in precision was observed with fluorescence lifetime data versus fluorescence intensity data [24].

In addition, our statistical analysis demonstrated that only physiological FLIM led to statistically significant FRET results without being influenced by nonspecific FRET. In this analysis, the temperature was fixed at 37°C, while CO_2 control was varied and both intensity and FLIM data were acquired. With physiological FLIM, the experimental group versus either negative control comparison had very small p-values ($\leq 4.0 \times 10^{-10}$), which suggested that molecular interactions were detected by FRET, while the comparison of the two negative controls gave a large p-value (0.93), which suggested that no nonspecific FRET between cerulean and citrine occurred. Without physiological conditions, significant nonspecific FRET did occur, as indicated by the statistically significant p-values from the comparison of the two negative controls for both FLIM and intensity data. On the other hand, due to their high variability, intensity-based measurements led to inconclusive results regarding the detection of molecular interactions [24].

Implementing FLIM with physiological conditions can significantly improve FRET detection, clearly and unambiguously indicating the presence of specific live-cell molecular interactions between RhoGDIγ and RhoC. The approach described here is generally applicable to improve the detection of FRET in a variety of live-cell systems.

6 Conclusions

In this chapter, we have discussed the concepts, the key features, the advantages, and several applications of FLIM. Compared to intensity-based methods, lifetime imaging requires less calibration and/or correction for fluorophore concentration variations, photobleaching, sources of optical loss, and other artifacts that affect fluorescence intensity measurements. Several applications of FLIM for quantitative, live cell imaging were presented, including studies of cellular metabolic pathways, improved FRET detection of oncogene association, microfluidic bioreactor characterization for continuous cell culture, and improved analysis of FLIM images including image restoration and precision enhancement. Continuing advances in microscopy technology and the increasing availability of commercial FLIM modules for confocal and multiphoton microscopes will likely make FLIM a critical research tool for cell and molecular biology.

Acknowledgments We would like to acknowledge technical contributions from and helpful discussions with Drs. Mei Wu, Sofia D. Merajver, Dhruv Sud, Wei Zhong, Paul Urayama, David G. Beer, Jennifer Linderman, Shuichi Takayama, and Geeta Mehta, as well as Karl A. Merrick, Khamir Mehta, Jonathon Girroir, and Joe Delli. This work was supported in part by funding from the National Institutes of Health (CA-112173, CA-77612, and CA-114542) and The Whitaker Foundation.

References

1. Lakowicz JR (2006) Principles of fluorescence spectroscopy, 3rd edn. Springer, Berlin
2. Chang CW, Sud D, Mycek MA (2007) Fluorescence lifetime imaging microscopy. Methods Cell Biol 81:495–524
3. Takanishi CL, Bykova EA, Cheng W, Zheng J (2006) GFP-based FRET analysis in live cells. Brain Res 1091(1):132–139
4. Tsien RY (1998) The green fluorescent protein. Annu Rev Biochem 67:509–544
5. Zal T, Gascoigne NR (2004) Photobleaching-corrected FRET efficiency imaging of live cells. Biophys J 86(6):3923–3939
6. Grant DM, McGinty J, McGhee EJ, Bunney TD, Owen DM, Talbot CB, Zhang W, Kumar S, Munro I, Lanigan PM, Kennedy GT, Dunsby C, Magee AI, Courtney P, Katan M, Neil MA, French PM (2007) High speed optically sectioned fluorescence lifetime imaging permits study of live cell signaling events. Opt Express 15(24):15656–15673
7. Kumar S, Dunsby C, De Beule PAA, Owen DM, Anand U, Lanigan PMP, Benninger RKP, Davis DM, Neil MAA, Anand P, Benham C, Naylor A, French PMW (2007) Multifocal multiphoton excitation and time correlated single photon counting detection for 3-D fluorescence lifetime imaging. Opt Express 15(20):12548–12561
8. Schlachter S, Elder AD, Esposito A, Kaminski GS, Frank JH, van Geest LK, Kaminski CF (2009) mhFLIM: resolution of heterogeneous fluorescence decays in widefield lifetime microscopy. Opt Express 17(3):1557–1570
9. Kuchibhotla KV, Lattarulo CR, Hyman BT, Bacskai BJ (2009) Synchronous hyperactivity and intercellular calcium waves in astrocytes in Alzheimer mice. Science 323(5918):1211–1215
10. Kotaleski JH, Blackwell KT (2010) Modelling the molecular mechanisms of synaptic plasticity using systems biology approaches. Nat Rev Neurosci 11(4):239–251
11. Marcu L (2010) Fluorescence lifetime in cardiovascular diagnostics. J Biomed Opt 15(1): 011106
12. Seefeldt B, Kasper R, Seidel T, Tinnefeld P, Dietz KJ, Heilemann M, Sauer M (2008) Fluorescent proteins for single-molecule fluorescence applications. J Biophotonics 1(1):74–82
13. Schweitzer D, Quick S, Schenke S, Klemm M, Gehlert S, Hammer M, Jentsch S, Fischer J (2009) Comparison of parameters of time-resolved autofluorescence between healthy subjects and patients suffering from early AMD. Ophthalmologe 106(8):714–722
14. Schweitzer D, Schenke S, Hammer M, Schweitzer F, Jentsch S, Birckner E, Becker W, Bergmann A (2007) Towards metabolic mapping of the human retina. Microsc Res Tech 70(5):410–419
15. Urayama P, Zhong W, Beamish JA, Minn FK, Sloboda RD, Dragnev KH, Dmitrovsky E, Mycek MA (2003) A UV-visible-NIR fluorescence lifetime imaging microscope for laser-based biological sensing with picosecond resolution. Appl Phys B 76(5):483–496
16. Zhong W, Wu M, Chang CW, Merrick KA, Merajver SD, Mycek MA (2007) Picosecond-resolution fluorescence lifetime imaging microscopy: a useful tool for sensing molecular interactions in vivo via FRET. Opt Express 15(26):18220–18235
17. Requejo-Isidro J, McGinty J, Munro I, Elson DS, Galletly NP, Lever MJ, Neil MAA, Stamp GWH, French PMW, Kellett PA, Hares JD, Dymoke-Bradshaw AKL (2004) High-speed wide-field time-gated endoscopic fluorescence-lifetime imaging. Opt Lett 29(19):2249–2251
18. Munro I, McGinty J, Galletly N, Requejo-Isidro J, Lanigan PM, Elson DS, Dunsby C, Neil MA, Lever MJ, Stamp GW, French PM (2005) Toward the clinical application of time-domain fluorescence lifetime imaging. J Biomed Opt 10(5):051403
19. Cano-Raya C, Ramos MDF, Vallvey LFC, Wolfbeis OS, Schaferling M (2005) Fluorescence quenching of the europium tetracycline hydrogen peroxide complex by copper(II) and other metal ions. Appl Spectrosc 59(10):1209–1216
20. Urayama PK, Mycek MA (2003) Fluorescence lifetime imaging microscopy of endogenous biological fluorescence. In: Mycek MA, Pogue BW (eds) Handbook of biomedical fluorescence. Marcel-Dekker, New York, pp 211–236

21. Sud D, Zhong W, Beer DG, Mycek MA (2006) Time-resolved optical imaging provides a molecular snapshot of altered metabolic function in living human cancer cell models. Opt Express 14(10):4412–4426
22. Xu Z, Raghavan M, Hall TL, Chang CW, Mycek MA, Fowlkes JB, Cain CA (2007) High speed imaging of bubble clouds generated in pulsed ultrasound cavitational therapy-histotripsy. IEEE Trans Ultrason Ferroelectr Freq Control 54(10):2091–2101
23. Pitts JD, Mycek MA (2001) Design and development of a rapid acquisition laser-based fluorometer with simultaneous spectral and temporal resolution. Rev Sci Instrum 72(7): 3061–3072
24. Chang CW, Wu M, Merajver SD, Mycek MA (2009) Physiological fluorescence lifetime imaging microscopy improves Förster resonance energy transfer detection in living cells. J Biomed Opt 14(6):060502
25. Bugiel I, König K, Wabnitz H (1989) Investigation of cell by fluorescence laser scanning microscopy with subnanosecond time resolution. Lasers Life Sci 3(1):47–53
26. Wang XF, Uchida T, Coleman DM, Minami S (1991) A two-dimensional fluorescence lifetime imaging system using a gated image intensifier. Appl Spectrosc 45(3):360–366
27. Sharman KK, Periasamy A, Ashworth H, Demas JN, Snow NH (1999) Error analysis of the rapid lifetime determination method for double-exponential decays and new windowing schemes. Anal Chem 71(5):947–952
28. Sud D, Mycek MA (2008) Image restoration for fluorescence lifetime imaging microscopy (FLIM). Opt Express 16(23):19192–19200
29. Chang CW, Mycek MA (2009) Improving precision in time-gated FLIM for low-light live-cell imaging. Proc SPIE 7370(2009):7370091–7370096
30. Vonesch C (2009) Fast and automated wavelet-regularized image restoration in fluorescence microscopy. PhD thesis, École Polytechnique Fédérale De Lausanne, Lausanne
31. Buranachai C, Kamiyama D, Chiba A, Williams BD, Clegg RM (2008) Rapid frequency-domain FLIM spinning disk confocal microscope: Lifetime resolution, image improvement and wavelet analysis. J Fluoresc 18(5):929–942
32. Buades A, Coll B, Morel JM (2005) A review of image denoising algorithms, with a new one. Multiscale Model Simul 4(2):490–530
33. Chang CW, Mycek MA (2010) Increasing precision of lifetime determination in fluorescence lifetime imaging. Proc SPIE 7570(2010):757007
34. Chang C-W, Mycek M-A (2010) Precise fluorophore lifetime mapping in live-cell, multi-photon excitation microscopy. Opt Express 18(8):8688–8696
35. Boulanger J, Sibarita JB, Kervrann C, Bouthemy P (2008) Non-parametric regression for patch-based fluorescence microscopy image sequence denoising. In: IEEE international symposium on biomedical imaging: from nano to macro, vols 1–4, pp 748–751
36. Delpretti S, Luisier F, Ramani S, Blu T, Unser M (2008) Multiframe SURE-LET denoising of timelapse fluorescence microscopy images. In: IEEE international symposium on biomedical imaging: from nano to macro, vols 1–4, pp 149–152
37. Gu W, Zhu XY, Futai N, Cho BS, Takayama S (2004) Computerized microfluidic cell culture using elastomeric channels and Braille displays. Proc Natl Acad Sci USA 101(45): 15861–15866
38. Dobrucki JW (2001) Interaction of oxygen-sensitive luminescent probes Ru(phen)(3)(2+) and Ru(bipy)(3)(2+) with animal and plant cells in vitro – mechanism of phototoxicity and conditions for non-invasive oxygen measurements. J Photochem Photobiol B Biol 65(2–3):136–144
39. Asiedu JK, Ji J, Nguyen M, Rosenzweig N, Rosenzweig Z (2001) Development of a digital fluorescence sensing technique to monitor the response of macrophages to external hypoxia. J Biomed Opt 6(2):116–121
40. Ji J, Rosenzweig N, Jones I, Rosenzweig Z (2002) Novel fluorescent oxygen indicator for intracellular oxygen measurements. J Biomed Opt 7(3):404–409
41. Castellano FN, Lakowicz JR (1998) A water-soluble luminescence oxygen sensor. Photochem Photobiol 67(2):179–183

42. Gerritsen HC, Sanders R, Draaijer A, Levine YK (1997) Fluorescence lifetime imaging of oxygen in living cells. J Fluoresc 7:11–16
43. Malak H, Dobrucki JW, Malak MM, Swartz HM (1998) Oxygen sensing in a single cell with ruthenium complexes and fluorescence time-resolved microscopy. Biophys J 74(2):A189
44. Lakowicz JR (1999) Principles of fluorescence spectroscopy. Kluwer Academic, New York
45. Zhong W, Urayama P, Mycek MA (2003) Imaging fluorescence lifetime modulation of a ruthenium-based dye in living cells: the potential for oxygen sensing. J Phys D Appl Phys 36(14):1689–1695
46. Kutala VK, Parinandi NL, Pandian RP, Kuppusamy P (2004) Simultaneous measurement of oxygenation in intracellular and extracellular compartments of lung microvascular endothelial cells. Antioxid Redox Signal 6(3):597–603
47. Sud D, Mycek MA (2009) Calibration and validation of an optical sensor for intracellular oxygen measurements. J Biomed Opt 14(2):020506
48. Sud D, Mehta G, Mehta K, Linderman J, Takayama S, Mycek MA (2006) Optical imaging in microfluidic bioreactors enables oxygen monitoring for continuous cell culture. J Biomed Opt 11(5):050504
49. Leclerc E, Sakai Y, Fujii T (2003) Cell culture in 3-dimensional microfluidic structure of PDMS (polydimethylsiloxane). Biomed Microdevices 5(2):109–114
50. Shiku H, Saito T, Wu CC, Yasukawa T, Yokoo M, Abe H, Matsue T, Yamada H (2006) Oxygen permeability of surface-modified poly(dimethylsiloxane) characterized by scanning electrochemical microscopy. Chem Lett 35(2):234–235
51. Mehta G, Mehta K, Sud D, Song JW, Bersano-Begey T, Futai N, Heo YS, Mycek MA, Linderman JJ, Takayama S (2007) Quantitative measurement and control of oxygen levels in microfluidic poly(dimethylsiloxane) bioreactors during cell culture. Biomed Microdevices 9(2):123–134
52. Urayama PK, Mycek MA (2003) Fluorescence lifetime imaging microscopy of endogenous biological fluorescence. In: Mycek MA, Pogue BW (eds) Handbook of biomedical fluorescence. Marcel Dekker, New York
53. Ramanujam N (2000) Fluorescence spectroscopy of neoplastic and non-neoplastic tissues. Neoplasia 2(1–2):89–117
54. Lakowicz JR, Szmacinski H, Nowaczyk K, Johnson ML (1992) Fluorescence lifetime imaging of free and protein-bound NADH. Proc Natl Acad Sci USA 89:1271–1275
55. Schneckenburger H, König K (1992) Fluorescence decay and imaging of NAD(P)H and flavins as metabolic indicators. Opt Eng 31(7):1447–1451
56. Georgakoudi I, Jacobson BC, Muller MG, Sheets EE, Badizadegan K, Carr-Locke DL, Crum CP, Boone CW, Dasari RR, Van Dam J, Feld MS (2002) NAD(P)H and collagen as in vivo quantitative fluorescent biomarkers of epithelial precancerous changes. Cancer Res 62(3):682–687
57. Förster T (1948) Intermolecular energy migration and fluorescence. Ann Phys (Leitzig) 2: 55–75
58. Kreiss P, Cameron B, Rangara R, Mailhe P, Aguerre-Charriol O, Airiau M, Scherman D, Crouzet J, Pitard B (1999) Plasmid DNA size does not affect the physicochemical properties of lipoplexes but modulates gene transfer efficiency. Nucleic Acids Res 27(19):3792–3798
59. Ross PC, Hui SW (1999) Lipoplex size is a major determinant of in vitro lipofection efficiency. Gene Ther 6(4):651–659
60. Schmid JA, Sitte HH (2003) Fluorescence resonance energy transfer in the study of cancer pathways. Curr Opin Oncol 15:55–64
61. Wallrabe H, Periasamy A (2005) Imaging protein molecules using FRET and FLIM microscopy. Curr Opin Biotechnol 16(1):19–27
62. Chen Y, Elangovan M, Periasamy A (2005) FRET data analysis: the algorithm. In: Periasamy A, Day RN (eds) Molecular imaging. Oxford University Press, New York, pp 126–145
63. Demarco IA, Periasamy A, Booker CF, Day RN (2006) Monitoring dynamic protein interactions with photoquenching FRET. Nat Methods 3(7):519–524

64. Hoppe A, Christensen K, Swanson JA (2002) Fluorescence resonance energy transfer-based stoichiometry in living cells. Biophys J 83(6):3652–3664
65. Chen Y, Mills JD, Periasamy A (2003) Protein localization in living cells and tissues using FRET and FLIM. Differentiation 71(9–10):528–541
66. Provenzano PP, Eliceiri KW, Keely PJ (2009) Multiphoton microscopy and fluorescence lifetime imaging microscopy (FLIM) to monitor metastasis and the tumor microenvironment. Clin Exp Metastasis 26(4):357–370
67. Yi YH, Ho PY, Chen TW, Lin WJ, Gukassyan V, Tsai TH, Wang DW, Lew TS, Tang CY, Lo SJ, Chen TY, Kao FJ, Lin CH (2009) Membrane targeting and coupling of NHE1-integrin{alpha} IIb{beta}3-NCX1 by lipid rafts following integrin-ligand interactions trigger Ca2+ oscillations. J Biol Chem 284(6):3855–3864
68. Chen Y, Periasamy A (2004) Characterization of two-photon excitation fluorescence lifetime imaging microscopy for protein localization. Microsc Res Tech 63(1):72–80
69. Vermeer JE, Van Munster EB, Vischer NO, Gadella TW Jr (2004) Probing plasma membrane microdomains in cowpea protoplasts using lipidated GFP-fusion proteins and multimode FRET microscopy. J Microsc 214(Pt 2):190–200
70. Ng T, Squire A, Hansra G, Bornancin F, Prevostel C, Hanby A, Harris W, Barnes D, Schmidt S, Mellor H, Bastiaens PI, Parker PJ (1999) Imaging protein kinase Calpha activation in cells. Science 283(5410):2085–2089
71. van Golen KL, Wu ZF, Qiao XT, Bao LW, Merajver SD (2000) RhoC GTPase, a novel transforming oncogene for human mammary epithelial cells that partially recapitulates the inflammatory breast cancer phenotype. Cancer Res 60(20):5832–5838
72. Holeiter G, Heering J, Erlmann P, Schmid S, Jahne R, Olayioye MA (2008) Deleted in Liver Cancer 1 Controls Cell Migration through a Dial-Dependent Signaling Pathway. Cancer Res 68(21):8743–8751
73. Hoppe AD, Shorte SL, Swanson JA, Heintzmannz R (2008) Three-dimensional FRET reconstruction microscopy for analysis of dynamic molecular interactions in live cells. Biophys J 95(1):400–418
74. Pertz O, Hodgson L, Klemke RL, Hahn KM (2006) Spatiotemporal dynamics of RhoA activity in migrating cells. Nature 440(7087):1069–1072
75. Semenova MM, Maki-Hokkonen AMJ, Cao J, Komarovski V, Forsberg KM, Koistinaho M, Coffey ET, Courtney MJ (2007) Rho mediates calcium-dependent activation of p38 alpha and subsequent excitotoxic cell death. Nat Neurosci 10(4):436–443
76. Hodgson L, Pertz O, Hahn KM (2008) Design and optimization of genetically encoded fluorescent biosensors: GTPase biosensors. Methods Cell Biol 85:63–81
77. Nakamura T, Aoki K, Matsuda M (2005) Monitoring spatio-temporal regulation of Ras and Rho GTPases with GFP-based FRET probes. Methods 37(2):146–153
78. Ahmed T, Shea K, Masters JRW, Jones GE, Wells CM (2008) A PAK4-LIMK1 pathway drives prostate cancer cell migration downstream of HGF. Cell Signal 20(7):1320–1328
79. Legg JW, Lewis CA, Parsons M, Ng T, Isacke CM (2002) A novel PKC-regulated mechanism controls CD44-ezrin association and directional cell motility. Nat Cell Biol 4(6):399–407
80. Parsons M, Monypenny J, Ameer-Beg SM, Millard TH, Machesky LM, Peter M, Keppler MD, Schiavo G, Watson R, Chernoff J, Zicha D, Vojnovic B, Ng T (2005) Spatially distinct binding of Cdc42 to PAK1 and N-WASP in breast carcinoma cells. Mol Cell Biol 25(5):1680–1695